International Journal of Nanomedicine

Dovepress
open access to scientific and medical research

Open Access Full Text Article

ORIGINAL RESEARCH

Enhancing Radiotherapeutic Effect With Nanoparticle-Mediated Radiosensitizer Delivery Guided By Focused Gamma Rays In Lewis Lung Carcinoma-Bearing Mouse Brain Tumor Models

This article was published in the following Dove Press journal:
International Journal of Nanomedicine

Sa-Hoe Lim[1,2]
Chun-Hao Li[3]
Young-Il Jeong[4]
Woo-Youl Jang[1,2]
Jin-Myung Choi[2]
Shin Jung[1,2]

[1]Department of Neurosurgery, Chonnam National University Medical School and Hwasun Hospital, Hwasun, Korea; [2]Brain Tumor Research Laboratory, Chonnam National University Research Institute of Medical Sciences, Chonnam National University Hwasun Hospital, Hwasun, Korea; [3]Department of Neurosurgery, Affiliated Hospital of Yanbian University, Yanji, Jilin 133000, People's Republic of China; [4]Biomedical Research Institute, Pusan National University Hospital, Pusan 602-739, Republic of Korea

Background: Targeting radiosensitizer-incorporated nanoparticles to a tumor could allow for less normal tissue toxicity with more efficient drug release, thus improving the efficacy and safety of radiation treatment. The aim of this study was to improve tumor-specific delivery and bioavailability of a nanoparticle-mediated radiosensitizer in mouse brain tumor models.

Methods: A pH-sensitive nanoparticle, chitoPEGAcHIS, was conjugated to recombinant peptide HVGGSSV that could bind to tax-interaction protein 1 (TIP-1) as a radiation-inducible receptor. Then the c-Jun N-terminal kinase (JNK) inhibitor, SP600125 was incorporated into this copolymer to fabricate a HVGGSSV-chitoPEGAcHIS-SP600125 (HVSP-NP) nanoradiosensitizer. In vitro and in vivo radiation treatment were performed using a Gamma Knife unit. The tumor targetability of HVSP-NP was estimated by optical bioluminescence. Synergistic therapeutic effects of radiation treatment and HVSP-NP were investigated in Lewis lung carcinoma (LLC) cell-bearing mouse brain tumor models.

Results: The SP600125 JNK inhibitor effectively reduced DNA damage repair to irradiated LLC cells. A pH sensitivity assay indicated that HVSP-NP swelled at acidic pH and increased in diameter, and its release rate gradually increased. Optical bioluminescence assay showed that radiation induced TIP-1 expression in mouse brain tumor and that the nanoradiosensitizer selectively targeted irradiated tumors. Radiation treatment with HVSP-NP induced greater apoptosis and significantly inhibited tumor growth compared to radiation alone.

Conclusion: As a novel nanoradiosensitizer, HVSP-NP was found to be able to selectively target irradiated tumors and significantly increase tumor growth delay in LLC-bearing mouse brain tumor models. This research shows that delivering a pH-sensitive nanoradiosensitizer to a brain tumor in which TIP-1 is induced by radiation can result in improved radiosensitizer-release in an acidic microenvironment of tumor tissue and in created synergistic effects in radiation treatment.

Keywords: brain neoplasms, radiotherapy, TIP-1 receptor, nanoparticles, radiosensitizer

Introduction

Metastatic brain tumor is the most common intracranial tumor in adults. Its incidence is 10-times more frequent than primary brain tumor.[1] As the survival rate of cancer patients has increased and medical diagnostic imaging has improved, patients with metastatic brain tumor have continued to increase. The most common treatment options for metastatic brain tumors include surgery, chemotherapy, radiotherapy, and their combination. Radiosurgery, such as Gamma Knife radiosurgery

Correspondence: Shin Jung
Department of Neurosurgery, Chonnam National University Hwasun Hospital, 322, Seoyang-ro, Hwasun-eup, Hwasun-Gun, Jeollanam-do 519-763, Republic of Korea
Tel +82-61-379-8588
Fax +82-61-379-7181
Email sjung@chonnam.ac.kr

submit your manuscript | www.dovepress.com
DovePress
http://doi.org/10.2147/IJN.S227894

(GKR), has become a reasonable alternative to conventional open surgery or traditional radiotherapy. It is an important option in the management of brain metastases. Although radiotherapy is regarded as one of the promising treatment options for cancers, various side-effects have been reported.[2–5] If the tumor is large, located in the brainstem, or adjacent to critical structures, a satisfactory therapeutic effect cannot be obtained due to insufficient treatment dose. To solve these problems, radiosensitizers have been used to improve the sensitivity of radiation in the tumor.[6,7] Enhancing the radiosensitivity of the tumor could enable fewer or more effective doses, improving the therapeutic outcome of radiotherapy. It has been reported that c-Jun N-terminal kinase (JNK) activity inhibition can enhance radiosensitivity and apoptosis of tumor cells.[8] JNK belongs to an evolutionarily conserved family of mitogen-activated protein kinases (MAPK). It can be activated by treating cells with cytokines (such as TNF and IL-1) and exposing cells to a variety of environmental stresses.[9] JNK participates in all types of cellular responses including cell death. It is also involved in phosphorylation of H2AX in irradiated cell.[10–12] JNK-specific inhibitor has been investigated as a radiosensitizer. It has synergistic effects in combination with radiotherapy or chemotherapy.[13–16] In a recent study, we have demonstrated that by blocking JNK signaling using SP600125, γH2AX expression is decreased and apoptosis is increased in irradiated lung and breast cancer cells.[17] SP600125 can be utilized as a radiosensitizer. Small molecule inhibitors such as SP600125 have no specificity against cancer cells and can spread out in the whole body. This is a significant constraint in applying those drugs to intracranial tumors due to their adverse effects on normal cells and tissues. Nano-medicine technology using nanoparticles, polymeric micelles, and polymer conjugates may overcome such limitation. Nanoparticle-mediated drug formulations can decrease drug related toxicity, provide tumor microenvironment-responsive drug release behavior, and enable improved anticancer activity for tumor tissues.[18,19] Furthermore, polymeric nanoparticles allow efficient drug transfer to tumor cells over blood–brain barrier (BBB, which inhibits penetration of bioactive molecules including anticancer agents and radiosensitizers), thereby enhancing drug sensitivity in the tumor.[20–23] Radiation can induce site-specific expression of receptors within the tumor. These radiation-inducible receptors might be targeted by peptides selected by phage display.[24–26] Irradiation of tumors is known to increase expression levels of TIP-1 receptor before the onset of apoptosis or cell death.[27–29] HAN's group has reported that increased expression of TIP-1 on cell plasma membrane is closely associated with invasive and metastatic potential of breast cancer cells.[27,29] HVGGSSV peptide can specifically bind to TIP-1 cell surface receptor. Elevated levels of TIP-1 are associated with resistance of cancer cells against radiation therapy.[27,28]

In the present study, we used Lewis lung carcinoma (LLC) cell-bearing mouse brain tumor model to investigate nanoparticulate radiosensitizer (nanoradiosensitizer) as a scaffold for establishing a radiation-guided drug delivery system. To increase radiation-specific delivery and improve tumor bioavailability, the nanoradiosensitizer was functionalized with HVGGSSV peptide that could specifically target TIP-1 receptor within irradiated tumors. HVGGSSV peptide-decorated nanoparticle was fabricated. HVGGSSV peptide was conjugated to the end of poly(ethylene glycol) (PEG) to synthesize HVGGSSV-PEG. HVGGSSV-PEG was then conjugated with chitosan to synthesize HVGGSSV-chitoPEG. Drug release from a nanoparticle can be accomplished by using bonds that are sensitive to hydrolytic degradation or pH.[30,31] To endow pH-sensitivity against nanoparticles, acetyl-histidine (AcHIS) was conjugated to the backbone of chitosan chain to synthesize HVGGSSV-chitoPEGAcHIS. Therefore, HVGGSSV-chitoPEGAcHIS copolymer has TIP-1 specific and pH-sensitive properties as a drug deliver carrier. Radiosensitizers including SP600125 can be incorporated into this copolymer, resulting in HVGGSSV-chitoPEGAcHIS-SP600125 (HVSP-NP). We assessed contribution of concomitant HVSP-NP administration in radiation treatment against mouse brain tumors. This approach was able to improve tumor-specific delivery and bioavailability of a radiosensitizer, delay tumor growth, and prolong mouse survival in radiated mouse brain tumor models.

Materials And Methods

Cell Culture And Treatment Protocol

A murine Lewis lung cancer (LLC) cell line was obtained from the American Type Culture Collection (ATCC; Manassas, VA, USA). Cells were cultured in Dulbecco's modified Eagle's medium (DMEM) supplemented with 10% fetal bovine serum (FBS) (both from Gibco-BLR, Gaithersburg, MD, USA) at 37°C in a 5% CO_2/95% air incubator. The LLC-Fluc cell line was transfected with a Lentiviral vector containing firefly luciferase gene. SP600125, a JNK inhibitor, was supplied by Sigma (St. Louis, MO, USA), constituted in

dimethyl sulfoxide (DMSO, 10 mM), and stored at −80°C. Cells were irradiated using a Gamma Knife system.[32,33] Cell exposure to SP600125 was performed 2 hours before gamma-irradiation.

Chemical Conjugation: Synthesis Of Radiation-Guided Peptide (HVGGSSV) And pH-Sensitive Copolymer (chitoPEGAcHIS)

Water-soluble chitosan (WSC, deacetylation degree>97%, M.W.=7,000 g/mol) was purchased from Kittolife Co. (Pyeongtaek, Gyeonggi-do, Korea). PEG-succinimidylglutarate (M.W.=3,400 g/mol) was purchased from Sunbio Co. (Seoul, Korea). N-acetyl-L-histidine (AcHIS), N-hydroxysuccinimide (NHS), N-(3-dimethylaminopropyl)-N'-ethylcarbodiimide hydrochloride (EDAC), chloroform, dimethyl sulfoxide (DMSO), and 3-(4,5-dimethylthiazol-2-yl)-2,5-diphenyltetrazolium bromide (MTT) were purchased from Sigma-Aldrich Chemical Co., USA. SP600125 was purchased from LKT Labs. Co., (Minnesota, USA). Dialysis membrane or dialysis device with a M.W. cutoff (MWCO) of 2,000 g/mol, 8,000 g/mol, or 12,000 g/mol were purchased from Spectrum/Por Lab., Inc. (CA, USA). Chlorin e6 (Ce6) was purchased from Frontier Scientific Inc. (Logan, UT, USA). Hexapeptide HVGGSSV was purchased from Peptron CO. Ltd. (Daejeon, Korea). All organic solvents and other chemicals were used as extra-pure grade.

After the copolymer capable of acting as a drug deliver carrier was prepared, Ce6 dye was conjugated or SP600125 was incorporated, resulting in functionalized nanoparticles. First, HVGGSSV-PEG conjugates were produced. Briefly, 0.1 mM of PEG-succinimidyl glutarate was dissolved in 5 mL DMSO. Then 1.2 equivalents of HVGGSSV in 5 mL of H_2O/DMSO mixtures (1/4, v/v) were added. This reaction was magnetically stirred for 24 hours. Reactants were then introduced into a dialysis tube (MWCO: 2,000 g/mol) and dialyzed against deionized water for 1 day with exchanges of water at 2 hour intervals to remove organic solvent and unreacted peptide. Following this, dialyzed solution was lyophilized for 2 days. The yield of product was about 96.9%. Yield=[Weight of product/(feeding weight of PEG +feeding weight of HVGGSSV)]×100. Thereafter, HVGGSSV-chitoPEG copolymer was produced. Briefly, 0.1 mM HVGGSSV-PEG conjugates dissolved in 5 mL DMSO was mixed with 180 mg of WSC in 10 mL H_2O/DMSO mixtures (1/4, v/v). This was magnetically stirred for 24 hours. After that, the mixture was introduced into a dialysis tube (MWCO: 8,000 g/mol). Dialysis was continued for 2 days with exchanges of water at 2–3 hours intervals to remove organic solvent and unreacted products. Following this, dialyzed solution was lyophilized for 3 days. The yield of product was higher than 98%. Yield=[Weight of product/(feeding weight of HVGGSSV-PEG conjugates+feeding weight of WSC)]×100. Finally, HVGGSSV-chitoPEGAcHIS copolymer was produced as a drug deliver carrier. Briefly, 78.8 mg AcHIS dissolved in 5 mL DMSO was mixed with equivalent amounts of EDAC and NHS to activate carboxylic acid of AcHIS. This was reacted for 24 hours by magnetic stirring. It was then mixed with 295 mg HVGGSSV-chitoPEG copolymer dissolved in 10 mL H_2O/DMSO mixtures (1/4, v/v). This reaction was further stirred for 24 hours. After that, the reactant was introduced into the dialysis tube (MWCO: 12,000 g/mol). Dialysis was continued for 2 days with exchanges of water at 2–3 hour intervals to remove organic solvent and unreacted products. Following this, dialyzed solution was lyophilized for 3 days. The yield of product was about 97.3%. Yield [Weight of product/(feeding weight of HVGGSSV-chitoPEG conjugates+feeding weight of AcHIS)]×100. The content of Ac HIS in the final product (HVGGSSV-chitoPEGAcHIS copolymer) was estimated to be 18.9% (w/w) using the following formula: Content of Ac HIS=[(Weight of final product-feeding weight of HVGGSSV-chitoPEG copolymer)/Weight of final product]×100. Ce6-conjugated HVGGSSV-chitoPEGAcHIS copolymer was produced for confirming drug delivery. First, 3 mg Ce6 was activated with an equivalent amount of EDAC/NHS system in 2 mL DMSO. This was added to 27 mg HVGGSSV-chitoPEGAcHIS copolymer in 5 mL H_2O/DMSO mixtures (1/4, v/v). This reaction was further stirred for 24 hours. After that, the reactant was introduced into the dialysis tube (MWCO: 12,000 g/mol). Dialysis was continued for 1 day with exchanges of water at 2–3 hour intervals to remove organic solvent and unreacted products, resulting in nanoparticles. Following this, dialyzed solution was lyophilized for 3 days. The content of Ce6 was calculated to be about 8.7% (w/w) based on measurement at 664 nm with a UV spectrophotometer (UV-1601, Shimadzu Co. Ltd. Osaka, Japan) using the following formula: Content of Ce6=[(Weight of final product-feeding weight of HVGGSSV-chitoPEGAcHIS copolymer)/Weight of final product]×100.

Fabrication Of SP600125 Incorporated pH-Sensitive Nanoradiosensitizer

HVGGSSV-chitoPEGAcHIS copolymers (45 mg) were distributed in 3 mL water with 20-second sonication (1s×20) using an ultra-sonicator (Sonics, VCX-750, Sonics & Materials Inc., CT, USA) and 4 mL of DMSO was added. SP600125 (5 mg) dissolved in 3 mL DMSO was then added and stirred for 20 minutes. The mixture was then introduced into a dialysis tube (MWCO=8,000 g/mol) and dialyzed against water for 1 day with exchange of distilled water at 3 hour intervals, resulting in HVGGSSV-chitoPEGAcHIS-SP600125 nanoparticle (HVSP-NP). Dialyzed solution was used for analysis or lyophilized for 3 days. Empty nanoparticles (E-NP) were fabricated in a manner similar to that described above, but without drug. To measure drug contents, 5 mg lyophilized solid was dissolved in DMSO and then stirred for 3 hours. PL contents were measured using a UV-spectrophotometer (UV-1601, Shimadzu Co. Ltd. Osaka, Japan) at 320 nm. Drug contents were calculated as follows: drug content (%, w/w)=(SP600125 weight/total weight of nanoparticle)×100. E-NP was used for blank test.

Analysis Using ^{1}H Nuclear Magnetic Resonance (NMR) Spectroscopy

A ^{1}H NMR spectrometer (500 mHz superconducting Fourier transform (FT)-NMR spectrometer, Varian Unity Inova 500 MHz NB High Resolution FT NMR; Varian Inc, Santa Clara, CA, USA) was used to monitor synthesis of HVGGSSV-chitoPEGAcHIS copolymers.

Characterization Of HVSP-NP Nanoradiosensitizer

HVSP-NP is a functional nanoparticulate radiosensitizer. Morphologies of nanomaterials were observed using a field-emission scanning electron microscope (S-4800; Hitachi, Tokyo, Japan) at 10 kV or 15 kV. Nanoparticle solution prepared as described above was dropped onto a cover slide and dried at room temperature for 6 hours. Particle size and zeta potential were measured using a Zetasizer Nano-ZS (Malvern, Worcestershire, UK). The concentration of nanoparticles was adjusted to be 0.1% (w/w).

A drug release test of HVSP-NP was performed. The dialyzed solution as described above was adjusted to 30 mL. Then 7 mL of this solution was placed into a dialysis membrane (MWCO: 12,000 g/mol). The dialysis membrane was then introduced into a 50 mL Falcon tube containing 43 mL phosphate-buffered saline (PBS, 0.01M, pH 7.4) and then agitated at 100 rpm (37°C). Whole media were taken to measure the released amount of SP600125 from nanoparticle (HVSP-NP) and then replaced with fresh media. The concentration of SP600125 was measured with a UV-spectrophotometer (UV-1601, Shimadzu Co. Ltd. Osaka, Japan) at 320 nm. E-NP was used for blank test. pH of media was adjusted to be 5~7.4 to investigate the effect of pH on drug release behavior.

MTT Assay

To assess the toxicity of HVSP-NP, cell metabolic activity was estimated using 3-(4,5-dimethylthiazol-2-yl)-2,5-diphenyltetrazolium bromide (MTT) assay. Briefly, LLC (10^3 cell/well) cells were seeded into 96-well plates and cultured in DMEM supplemented with 10% FBS at 37°C in 5% CO_2/95% air. Different concentrations (100, 50, 25, 12.5, 6.25, 3.125, 0 M) of SP600125 in DMEM were then added into each well. After 24 hours, 0.5 mg/mL MTT solution was added into each well and incubated for 1 hour. The supernatant was then removed from each well and 100 μL DMSO was added to dissolve MTT formazan. Optical density was determined by measuring absorbance at 540 nm.

Mouse Brain Tumor Modeling And Treatment Conditions

All animal experiments were performed in accordance with an ethical and legal approved protocol by the Institutional Animal Care and Use Committee at Chonnam National University Gwangju, Korea (approval number: CNU IACUC-H-2017-54). C57BL/6 female mice at 7 weeks old were obtained from OrientBio (Seongnam, Republic of Korea). LLC-Fluc cells (2×10^5) were diluted in 3 μL PBS and stereotactically inoculated (1 μL/min) into mouse brain. Cell line infusion site was located by identifying the intersection of sagittal and coronal sutures to define bregma and then measuring 2 mm right lateral and 1 mm posterior of the bregma. Injection depth was adjusted to 3 mm. Nanoparticles were given by tail vein injection without premedication.

Western Blotting And Immunohistochemistry (IHC)

Western blotting was conducted according to the protocol established in previous studies.[17,34,35] Briefly, harvested cells were lysed with RIPA buffer containing Tris-HCl (pH 7.5), 1% Triton X-100, 0.15 M NaCl, 0.5% sodium deoxycholate, and 2 mM EDTA (Bio-solution). Proteins

extracted from whole cell lysates (30 μg) were subjected to electrophoresis using 10% SDS-polyacrylamide gel at 100 V for 2 hours and then transferred to PVDF membranes at 100 V for 1 hour on ice. Membranes were blocked with 5% non-fat dry milk for 1 hour at room temperature, incubated with following primary antibodies at 4°C overnight: GAPDH (1:2,000, CST), anti-TIP-1 (1:5,000; Abcam), p-JNK (1:200; Santa Cruz Biotechnology), and phospho-histone H2AX (Ser139) rabbit monoclonal antibodies (1:1,000, CST). A horseradish peroxidase-conjugated goat anti-rabbit IgG (1:3,000; CST) was used as a secondary antibody. Protein detection and levels were determined using Amersham imager 600 (Amersham Biosciences).

IHC was carried out as previously described.[36,37] Briefly, brains were removed from sacrificed mice, fixed with 10% formaldehyde solution, and then used to prepare paraffin-embedded block. Consecutive 3 μm-thick tissue sections from blocks were then transferred to poly-L-lysine-coated slides for IHC analysis. Slides were dewaxed in xylene for 15 minutes, hydrated with ethanol solution series of low concentration (60%, 80%, 100%) for 10 minutes, and then washed with distilled water for 10 minutes. For IHC staining with γ-H2AX and TIP-1, slides were subjected to heat-induced epitope retrieval that involved pre-heating using high pressure and EnVision FLEX Target Retrieval low pH solution (Dako). Endogenous peroxidase activity was quenched by peroxidase-blocking solution (Dako) for 30 minutes. Non-specific protein binding was blocked with antibody diluent solution (Dako) for 30 minutes. Primary antibodies used for staining were as follows: rabbit Anti-TIP-1 antibody (1:100; Abcam) and rabbit phospho-histone H2AX (Ser139) antibody (1:500; Cell Signaling). Primary antibody was added and incubated at 4°C overnight. After washing with PBST, ImmPRESS universal reagent anti-mouse/rabbit Ig (Vector laboratories, Inc.) was used as a secondary antibody and incubated with samples at room temperature for 1 hour. After washing with PBST, DAB (Vector laboratories, Inc.) was added and the reaction was stopped by washing as soon as the color changed to brown. Harris hematoxylin was used for counterstaining.

Bioluminescence Imaging

Bioluminescence images (BLI) of the mouse brain tumor were acquired with a Night Owl In Vivo Imaging System (Berthold technologies, Bad Wildbad, Germany). Anesthetized mice with isoflurane (2.5% in air) were placed in the system. Then 3 mg D-luciferin (PerkinElmer) was intraperitoneally injected into each mouse. Photons emitted from the tumor expressing luciferase were collected for 2 minutes. Pseudo-color images indicating photon counts were analyzed using IndiGo software (Berthold technologies).

Statistical Analyses

Descriptive statistics are presented as mean±standard deviation (SD) or range. Independent-samples *t*-test was used for between-group comparisons. All statistical analyses were performed using SPSS version 19.0 (SPSS Inc., Chicago, IL, USA), with significance level set at $P<0.05$.

In Vitro And In Vivo Irradiation Conditions

LLC cultures were irradiated using dedicated in vitro apparatus for Leksell Gamma Knife (LGK). Cultured cells were placed at $6*10^6$ cells/tube in conical culture tubes and then centrifuged. They were collected at the bottom of the tube to form a constant target volume. Radiation dose was adjusted using Leksell GammaPlan (LGP). Mouse brain tumor was also irradiated with LGK. The mouse was positioned on a dedicated adaptor for small animal and its head midline was aligned to the center axis of the adaptor. Fractionated radiation was exposed to mouse brain. Radiation dose applied to the mouse was computed on the basis of a linear quadratic model. Biologically effective dose (BED) was calculated with the following equation:

$$\mathrm{BED} = \mathrm{nd} \times \left(1 + \frac{d}{\alpha/\beta}\right).$$

Where n was the number of fractions and d was the dose/fraction. α/β ratio was assumed to be 3 Gy for late-responding tissues such as brain and 10 Gy for early-responding tissues such as tumors.[38]

Results

Synthesis And Characterization Of HVSP-NP

To synthesize HVGGSSV-chitoPEGAcHIS copolymer, amine end group of HVGGSSV hexapeptide was conjugated with PEG-succinimidyl glutarate as shown in Figure 1A. Specific peaks of peptide were confirmed at 2.6–3.0 ppm, 6.8 ppm, and 7.5 ppm, while ethylene protons of PEG were confirmed at 3.4 ppm. Basically, HVGGSSV-PEG-g-chitosan copolymer was designed to become 10 molecules of HVGGSSV-PEG against 100 glucosamine. At ^{1}H NMR results, (1H, 4) proton of

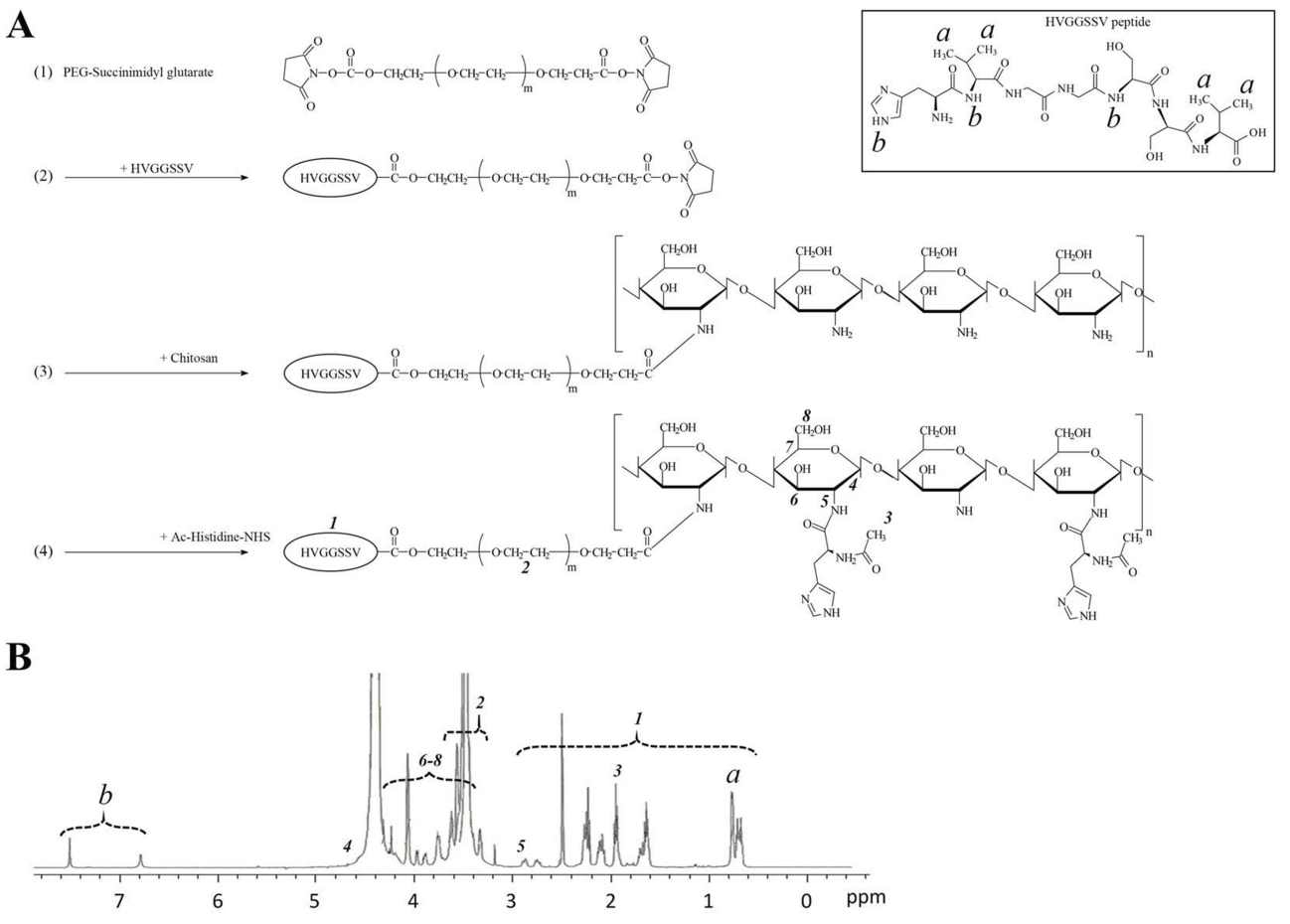

Figure 1 Synthesis of HVGGSSV-chitoPEGAcHIS copolymer having TIP-1 specific and pH-sensitive properties as SP600125-drug deliver carrier. (**A**) Synthesis scheme and chemical structure of HVGGSSV-chitoPEGAcHIS copolymer. (**B**) ^{1}H NMR spectrum of HVGGSSV-chitoPEGAcHIS copolymer.

glucosamine and ethylene proton of PEG appeared at 4.2~4.4 ppm and 3.4~3.5 ppm, respectively. From these results, proton of 1H and ethylene proton was compared to estimate substitution degree (DS) of HVGGSSV-PEG in HVGGSSV-chitoPEG copolymer. The number of DS of PEG versus 100 glucosamine was about 9.2. HVGGSSV-PEG conjugates were further conjugated with WSC and then AcHIS was attached to the backbone of chitosan to endow pH-sensitivity. ^{1}H NMR spectra of HVGGSSV-chitoPEGAcHIS copolymer are shown in Figure 1B. Specific peaks were confirmed at 1.6~2.6 ppm for acetyl histidine and at 3.2~4.2 ppm for chitosan. These results indicated that HVGGSSV-chitoPEGAcHIS copolymer was successfully synthesized.

As a pH-sensitive nanoradiosensitizer, HVSP-NP was prepared with sonication and dialysis procedure as described above. E-NP was prepared similarly in the absence of SP600125. As shown in Figure 2A, SEM photos indicated that E-NP and HVSP-NP had sphere-like shape and small particle sizes of less than 100 nm and 200 nm, respectively. Properties of particles were measured. Results are shown in Table 1.

Since HVSP-NP has pH-sensitivity, particle size changes were measured by pH variation, as shown in Figure 2B. Particle sizes of both E-NP and HVSP-NP were gradually increased at acidic pH. Their average sizes at pH 5 were at least 3-times larger than those at pH 7.4. These results indicated that HVSP-NP was swelled at acidic pH and its diameter was increased. HIS group of chitosan backbone was composed of hydrophobic core of nanoparticles due to hydrophobicity of HIS moiety. However, hydrophobic properties of HIS were relatively hydrophilic in acidic media and then nanoparticles were swelled in the acidic environment. Figure 2C shows drug release behavior from HVSP-NP. As shown in Figure 2C-top, higher drug contents in nanoparticles resulted in slower release from nanoparticles. These results might be due to the fact that hydrophobic drug is easily aggregated in the core of nanoparticles with high drug contents, causing the drug to be dissolved slowly compared to

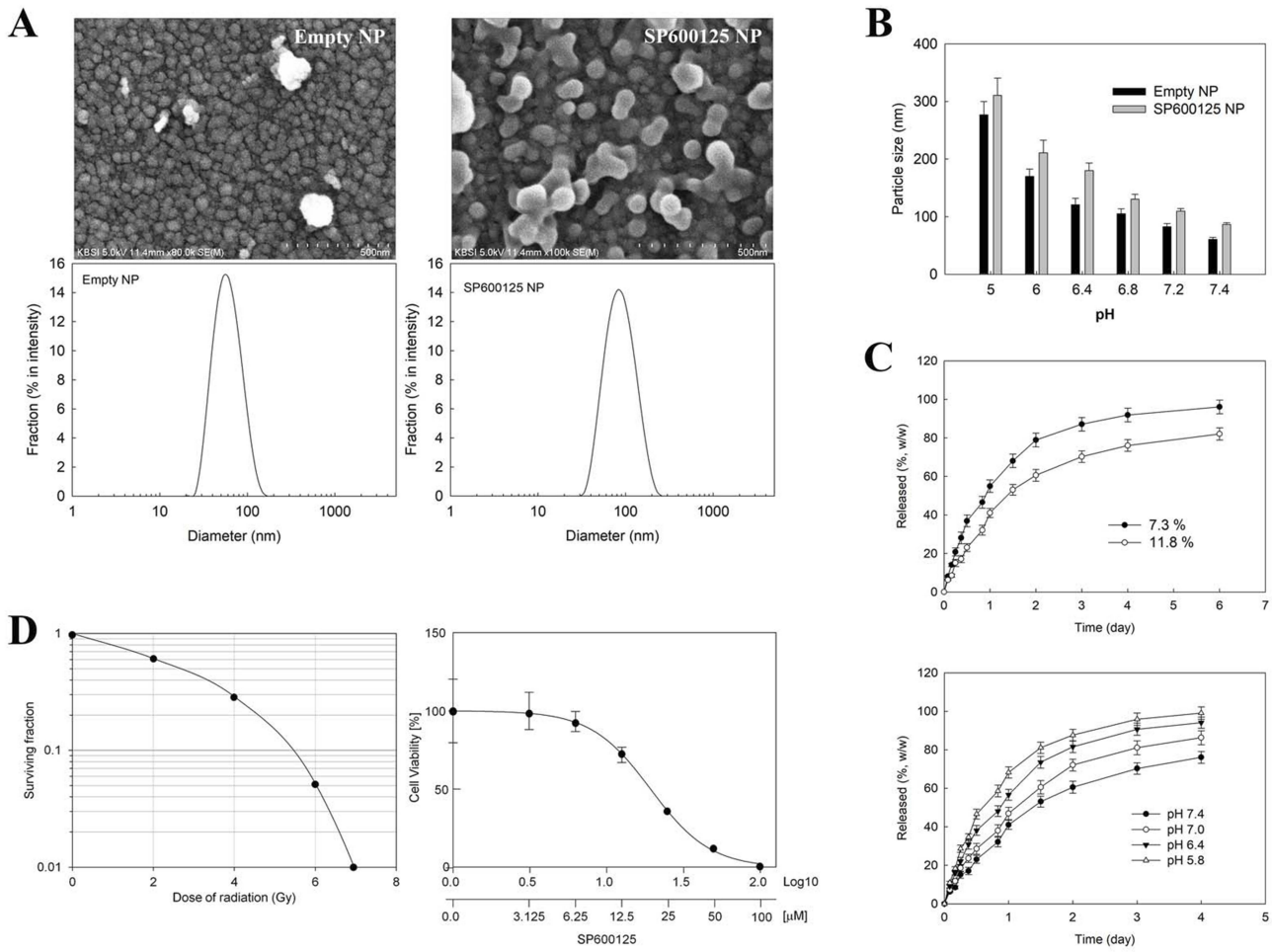

Figure 2 Characterization of HVSP-NP nanoparticle. (**A**) Morphology and particle size of empty nanoparticles and SP600125-incorporated nanoparticles. (**B**) Changes of nanoparticle size according to pH variations. (**C**) Drug release rate of HVSP-NP according to drug contents (top) and according to pH of media (bottom). (**D**) Survival curve derived from clonogenic-radiosensitivity assay of LLC cells treated with a dose of 2, 4, 6, 8, and 10 Gy (left); HVSP-NP dose-response curve derived from MTT-toxicity assay according to SP600125 contents in LLC cells (right).

nanoparticles with lower drug contents. The effect of pH on drug release rate from nanoparticles was also assessed by changes of media pH as shown in Figure 2C-bottom. Drug release rate from nanoparticles was gradually increased at acidic pH. These results were due to the fact that nanoparticles were swelled in acidic solution with increased diameters of nanoparticles, resulting in increased drug release.

Responses Of LLC Cell Line To Irradiation And HVSP-NP

To verify cellular radiation response of LLC cell lines to focused gamma beam of LGK driven-in vitro apparatus, cell survival curve was plotted on a log-linear scale with dose on the linear x-axis using clonogenic assay (Figure 2D-left). Survival curves for mammalian cells are usually presented in the form shown in this plot.

Table 1 Drug Contents And Particle Size Of HVSP-NP Nanoradiosensitizer

Nanoparticles	Polymer/Drug [w/w]	Drug Contents [%, w/w]		Particle Size [nm]*
		Theoretical	Experimental	
E-NP	50/0	—	—	57.6±2.8
HVSP-NP I	45/5	10	7.3	80.3±4.1
HVSP-NP II	45/10	18.2	11.2	118.4±20.8

Note: *Particle size results were average SD from three different samples.

The survival curve on the log-linear plot starts out straight with a finite initial slope at low doses, bends at higher doses, and tends to straighten again at very higher doses.[39] This in vitro apparatus showed good performance in verifying radiation response of cell line to gamma ray exposure. MTT assay results showed that the optical density of LLC cells was dose-dependently decreased after treatment with HVSP-NP (Figure 2D-right). The IC_{50} value of this radiosensitizer was calculated to be 19.26 μM (R^2=0.96).

Targeting The Nanoradiosensitizer To Radiation-Inducible Receptors Improved Tumor-Specific Drug Delivery

TIP-1 is a radiation-inducible antigen on the surface of tumor cells that can bind peptide ligand HVGGSSV. Western blotting was carried out to determine TIP-1 expression in irradiated LLC (Figure 3A). In the samples irradiated with 8 Gy, the highest induction of TIP-1 was observed at 16 hours after irradiation, while it was mildly reduced at 24 hours post-irradiation (Figure 3A-upper left). After 16 hours of irradiation, the degree of TIP-1 expression was assessed according to irradiation doses. Results showed that the amount of TIP-1 expression was increased as radiation dose increased (Figure 3A-upper right). Relative band quantification was determined by ImageJ, by normalizing to loading control, GAPDH. Histograms (below Western blot) reveal TIP-1 expression levels (abbreviations: n.s., not significant by Log rank test; *P<0.05). Error bars represent mean±standard deviation (SD). IHC staining also revealed higher levels of TIP-1 protein in irradiated tumors than those in untreated controls (Figure 3B). Each immunoreactivity pattern was evaluated by quadruplicate specimens from the same mouse. Scale bar, 10 μm.

An IVIS optical imaging study was conducted to determine whether targeting the nanoradiosensitizer to radiation-inducible receptors could improve tumor-specific drug delivery. We synthesized HVGGSSV-chitoPEGAcHIS copolymer by conjugating HVGGSSV peptide to pH-sensitive nanoparticles. This copolymer was then labeled with a fluorescent probe (Ce6) for in vivo fluorescence imaging studies. Figure 3C shows the IVIS study timeline to identify tumor targetability of HVSP-NP. Mice were classified into four categories of control, untreated (0 Gy), single fraction (2 Gy), and multi fraction (10 Gy=6.2 Gy*2). Bioluminescence images of mice were acquired at 10 days post-LLC cell injection. Mice bearing LLC brain tumors were treated with 0 Gy, 2 Gy, or fractionated 10 Gy (6.2 Gy×2) and administered HVGGSSV-chitoPEGAcHIS labeled with Ce6 (0.2 mg). As shown in Figure 3D, the bioluminescence images were reacquired at 7 days post-treatment. Tumor growth of radio-treated mice (2 Gy or f.10 Gy) was delayed compared to that of untreated (0 Gy) control mice. Fluorescence images were acquired and Ce6 dye signals were measured to verify drug delivery to the tumor. Irradiated tumor models showed greater radiance compared to untreated (0 Gy) control. Radiance increased as radiation dose increased (2 Gy and f.10 Gy). Histograms show the intensity of dye fluorescence (abbreviations: n.s., not significant by Log rank test; *P<0.05). Error bars indicate ±SD; columns, mean. In addition, the tumor within brain section was verified by H&E staining. It was then immunostained with TIP-1 antibody. Minimal staining of normal tissue and substantially increased staining of tumor cells were observed (Figure 3E). The level of TIP-1 increased more in tumor than in normal tissues, and non-specific stain was observed in the brain cortex. These results revealed that targeting HVGGSSV-conjugated nanoradiosensitizer to radiation-inducible receptor (TIP-1) could improve tumor-specific drug delivery.

Targeted Nanoradiosensitizer Enhances Therapeutic Efficacy In Mouse Brain Tumor Model

The synergy effect of HVSP-NP with radiation treatment was investigated by survival assay, in which LLC cell-bearing mouse brain tumor models were grouped (n=8) as control, HVSP-NP alone, RT alone, and RT with HVSP-NP. Figure 4A shows representative mouse brain MRI (T1 enhanced) in control, RT alone, and RT with HVSP-NP groups. MRI was scanned at 7 days after cell injection and 12 days after treatment. Tumor growth rate was measured to be 7.57 for control, 4.85 for RT alone, and 2.55 for RT with HVSP-NP. Tumor volume was measured using Leksell GammaPlan® (LGP, Dedicated treatment planning tool specifically designed for stereotactic radiosurgery). This result revealed that HVSP-NP delayed tumor growth in radiation treatment of mouse brain model. As shown in Figure 4B, survival assay was performed with Kaplan–Meier curve (abbreviations: n.s., not significant by Log rank test; *P<0.05; ***P<0.0001). The group treated with only HVSP-NP did not noticeably affect the survival of mice, whereas the radiation treatment group

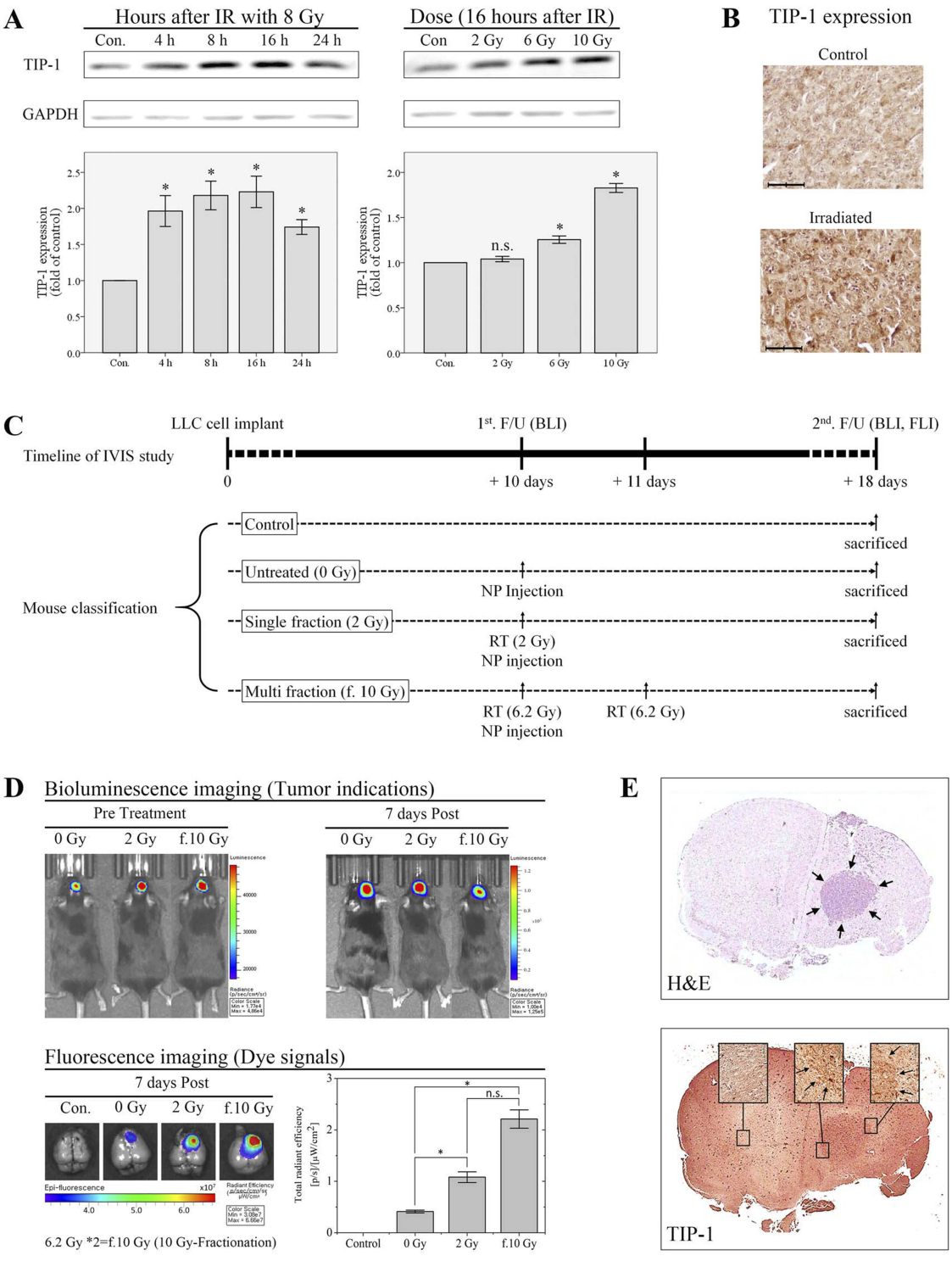

Figure 3 Radiation-inducible TIP-1 receptor targeting studies. (**A**) Western blotting analysis for TIP-1 expression at the time points indicated after irradiation with 8 Gy (left) and that after 16 hours at irradiation dose intervals indicated (right). Histograms show TIP-1 expression levels relative to the control. GAPDH was used as the internal control. Error bars indicate ±SD; columns, mean. (**B**) IHC staining with anti-TIP-1 antibody of untreated control and irradiated tumor. Each immunoreactivity pattern was confirmed by quadruplicate specimens from the same mouse. Scale bar, 10 μm. (**C**) Timeline of IVIS study to identify tumor targetability of HVSP-NP. Mice were classified into four categories of control, untreated (0 Gy), single fraction (2 Gy), and multi fraction (10 Gy=6.2 Gy*2). (**D**) IVIS optical imaging study to confirm whether targeting the nanoradiosensitizer to radiation-inducible receptors. Bioluminescence images of mice treated with Ce6-labeled nanoparticle (0.2 mg) and irradiation show tumor indications (upper-right) and fluorescence images of extracted mouse brains show Ce6 dye signals (lower-left). Histograms show the intensity of dye fluorescence. Error bars indicate ±SD; columns, mean. (**E**) Irradiated mouse brain section stained with H&E (upper) and with anti-TIP-1 antibody. Arrows indicate tumor margins. The level of TIP-1 increased more in tumor than in normal tissues, and non-specific stain was observed in the brain cortex.

Note: *P<0.05.

Abbreviations: n.s., not significant by Log rank test; F/U, follow-up; BLI, bioluminescence imaging; FLI, fluorescence imaging; NP injection, tail vein injection of Ce6-labeled nanoparticle; RT, radiation treatment.

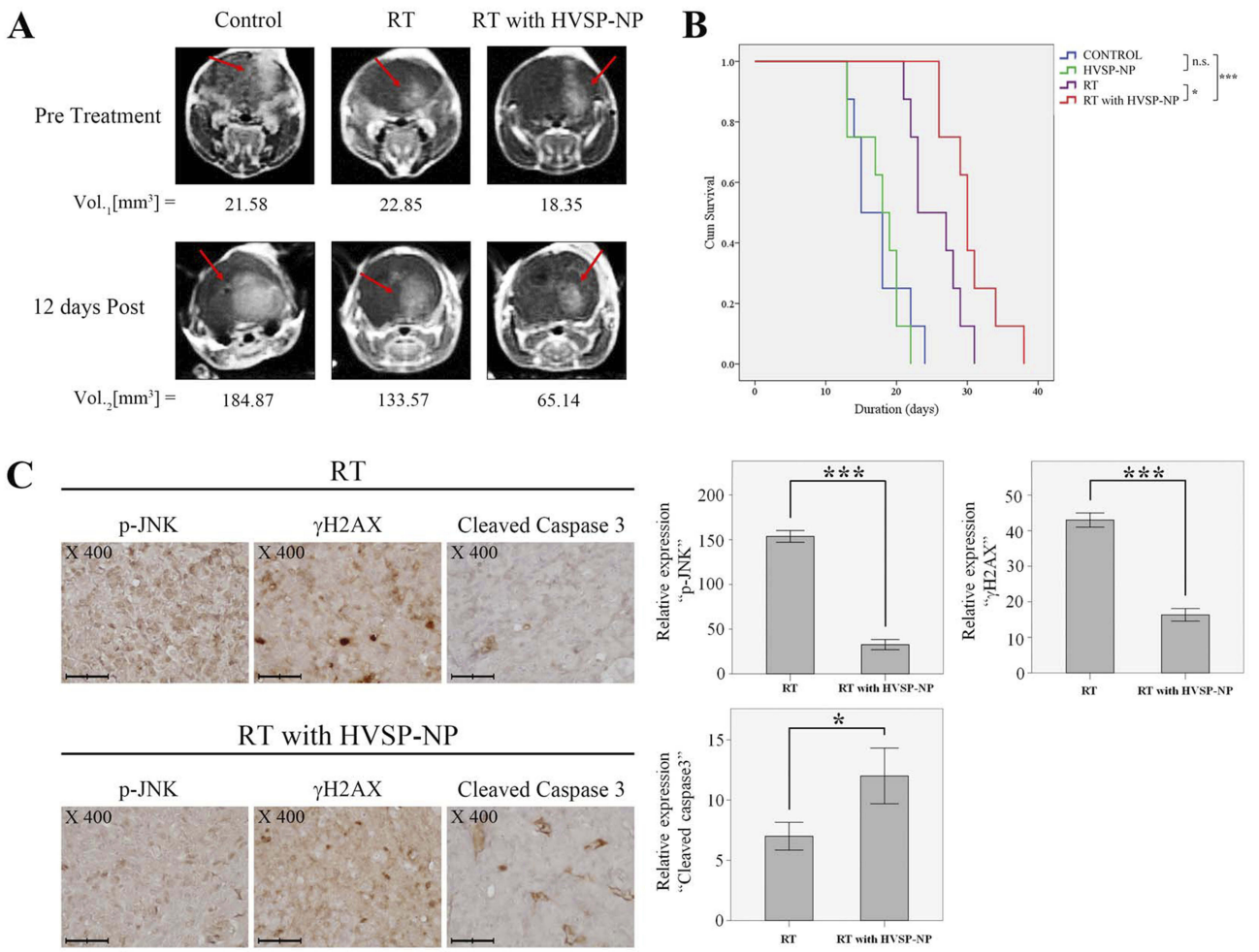

Figure 4 Survival studies for mice receiving various treatments. (**A**) MRI follow-up images. Tumor volume was measured using Leksell GammaPlan® (LGP, Dedicated treatment planning tool specifically designed for stereotactic radiosurgery). Red arrows indicate the presence of tumors. (**B**) Kaplan-Meier survival curves. (**C**) Immunohistochemistry staining results for p-JNK, γH2AX, and Cleaved Caspase-3 in extracted mouse brain tumors. Each immunoreactivity pattern was confirmed by quadruplicate specimens from the same mouse. Scale bar, 10 μm. Histograms showing the quantitative analysis of p-JNK, γH2AX and Cleaved Caspase3 expression levels for RT ± HVSP-NP. Error bars indicate ±SD; columns, mean.

Notes: **P*<0.05; ****P*<0.001.

Abbreviation: n.s., not significant by Log rank test.

significantly prolonged the survival compared to other groups. Especially, combination of radiation and HVSP-NP significantly (P=0.03) prolonged the survival compared to RT alone. To verify the effect of HVSP-NP on irradiated mouse brain tumor, tumor sections were immunostained for p-JNK, γH2AX, and Cleaved Caspase 3 (Figure 4C). Each immunoreactivity pattern was confirmed by quadruplicate specimens from the same mouse. Scale bar, 10 μm. In radiation-induced cells, JNK signalings are known to mediate the phosphorylation of H2AX. RT with HVSP-NP treatment induced a decrease in p-JNK and γH2AX expression compared to RT alone. To evaluate the mechanism of cell death, tumor sections were also immunostained for cleaved caspase-3 expression as an apoptosis marker. RT with HVSP-NP treatment produced greater apoptosis compared to RT alone. The histograms show the quantitative analysis of p-JNK, γH2AX, and cleaved Caspase3 expression levels for RT alone and RT with HVSP-NP (abbreviations: n.s., not significant by Log rank test; *P<0.05). Error bars indicate ±SD; columns, mean. These results suggest that HVSP-NP can suppress repair of cell damage by inhibiting p-JNK, eventually inducing more apoptosis.

Discussion

The prescription dose of radiation surgery is limited by the location or size of the tumor. Even if the tumor is under the critical boundary condition, an improved therapeutic effect can be expected while minimizing side-effects with relatively small doses by modulating radiation sensitivity

of the tumor. However, most radiosensitizers have no targetability against cancer cells. They spread throughout the whole body. That is, a radiosensitizer-drug without sufficient tumor selectivity can compromise drug efficacy and induce undesired side-effects. Tumor-specific drug delivery systems have been investigated using various targeting mechanisms, in which peptides, aptamers, antibodies, antigens, and so on are subjects of studies.[40,41] Particularly, since peptide has various characteristics including high affinity, lower molecular weight, lack of immunogenicity, and absorption by tumor cells, it has been extensively studied as a targeted drug carrier.[42,43] HVGGSSV peptide can distinguish irradiated tumors from untreated tumors and normal tissues, suggesting that this peptide has high potential in radiation-guided drug delivery to the tumor.[44,45] HVGGSSV has been actively studied as a tumor-targeting peptide that is capable of binding to radiation-induced receptors. HVGGSSV peptide can bind to TIP-1 receptors within a tumor and irradiation can be used to induce site-specific of these receptors.[25] These peptides can then be modified with cytotoxic drug-incorporated nanoparticles to establish radiation-guided drug delivery systems.[24] The nanomedicine delivery system based on receptor expression and stimuli in tumor cells has been extensively studied due to its superiorities in targeting specific tissues with minimized normal tissue toxicity.[46–50] Since tumor microenvironment causes various abnormal changes unlike normal tissues, these mechanisms can be investigated and applied to a nanomedicine drug delivery system.[51,52] Folate receptor in cancer cells enables folic acid-decorated nanoparticles to concentrate anticancer agents in the tumor. Carcinogenic receptors such as CD44 also enable nanoparticles to target cancer cells with minimized delivery of anticancer drugs to normal cells. Abnormal changes of the tumor microenvironment such as acidic pH and increased redox-potentials have also been investigated for stimuli-sensitive nanomedicines.[53–57] pH-sensitive nanoparticles can be used to release anticancer agents specifically in acidic environments of tumor tissues since normal cells and tissues maintain a weak basic physiological status.[58–60] For example, Lee et al[55] reported that Ac-HIS conjugated nanoparticles were swelled or partially disintegrated in the acidic pH. Furthermore, the diameter and surface charge of their nanoparticles were increased according to the acidity of aqueous solution. This behavior of nanoparticles induced a faster drug release rate at acidic pH than that in neutral or basic pH. Furthermore, Raja et al[61] reported that Ac-His-conjugated chitosan nanoparticles showed the acidic pH-triggered aggregation and disassembling properties. They also argued that drug release rate was accelerated in the acidic pH due to the pH-sensitivity of Ac-His and then efficiently suppressed breast tumor cells in vitro. We also observed that the diameter of nanoparticles was increased and then the drug release rate was also increased at acidic pH, ie, increase of nanoparticle surface at acidic pH may induce the opportunity of drug liberation from nanoparticles. Thie behavior of AcHIS-conjugated nanoparticles induced faster drug release in the acidic pH environment of the tumor. In this research, we tried to establish an intelligent radiosensitizer (HVSP-NP) delivery system based on radiation-guided peptide HVGGSSV and chitoPEGAcHIS nanoparticle sensitive to acidity (pH). We also assessed its synergy effect with radiotreatment. This approach can provide a means to target radiosensitizer specifically to irradiated brain tumor and to release this drug continuously in peritumoral environment. We have already revealed that SP600125 can increase the radiosensitivity in an irradiated subcutaneous tumor model.[17] The current study was intended for a LLC-cell bearing mouse brain tumor model, focusing on tumor specific delivery of HVSP-NP as a radiosensitizer. In these brain models, even though nanoparticles can be given by tail vein injection, this condition alone remains difficult for nanoparticles to be delivered into the brain because of the BBB. Although the integrity of BBB establishes a stable internal environment of the brain, BBB can be disrupted by osmotic disruption, bradykinin, or irradiation.[62] Therefore, focused gamma ray irradiation will cause tumor cell kill and may improve BBB penetration of HVSP-NP. NMR spectroscopy revealed that drug deliver carrier HVGGSSV-chitoPEGAcHIS was successfully synthesized. SP600125 was incorporated to this carrier and its characteristics were evaluated. Two forms of HVSP-NP with different particle sizes and drug contents were obtained: (1) HVSP-NP I with a size of 80.3±4.1 nm and a drug content of 7.3%; and (2) HVSP-NP II with a size of 118.4±20.8 nm and a drug content of 11.2%. Particle sizes of HVSP-NP I and II showed a monomodal distribution pattern. Experimental drug loading was lower than the theoretical one because SP600125 was liberated during the dialysis procedure. As a result of drug release test and particle swelling evaluation, drug release rate from nanoparticles was gradually increased at acidic pH, presumably because nanoparticles were swelled in the acidic solution and then increased

diameters of nanoparticles which resulted in increased drug release. This finding suggests that in a peritumoral microenvironment where acidity is increased, drug can be effectively released from the nanoparticle. We found that nanoradiosensitizer HVSP-NP could specifically target irradiated mouse brain tumors in our in vivo evaluation. This result shows that radiation can be utilized to induce the expression of TIP-1 within tumor microvasculature and significantly enhance the delivery of nanoparticles to the tumor site. Thus, conjugation with HVGGSSV can advance intratumoral biodistribution of nanoradiosensitizer and enhance tumor bioavailability, resulting in improved brain tumor growth delay. Furthermore, mouse survival assay confirmed that radiation treatment with a nanoradiosensitizer could significantly improve tumor growth delay compared to radiation treatment alone.

Conclusion

Our study shows that intelligent radiosensitizer HVSP-NP has intratumoral TIP-1 specific and pH-sensitive properties as a radiosensitizer deliver carrier and that its synergy with radiation treatment can improve brain tumor growth delay in in vivo assay. Recently, radiosurgery is used as an alternative to conventional craniotomy. Simultaneous treatment with nanoradiosensitizers may be another option to improve efficacy of high energy radiation and enhance cure rates for brain tumors.

Acknowledgements

This study was supported by a grant (HCRI17908-1) of Chonnam National University Hwasun Hospital Biomedical Research Institute.

Disclosure

The authors report no conflicts of interest in this work.

References

1. Nabors LB, Ammirati M, Bierman PJ, et al. Central nervous system cancers. *J Natl Compr Canc Netw*. 2013;11(9):1114–1151. doi:10.6004/jnccn.2013.0132
2. Hua L, Wang Z, Zhao L, et al. Hypoxia-responsive lipid-poly-(hypoxic radiosensitized polyprodrug) nanoparticles for glioma chemo- and radiotherapy. *Theranostics*. 2018;8(18):5088–5105. doi:10.7150/thno.26225.eCollection2018
3. Skiba-Tatarska M, Kusa-Podkanska M, Surtel A, Wysokinska-Miszczuk J. The side-effects of head and neck tumors radiotherapy. *Polski Merkuriusz Lekarski*. 2016;41(241):47–49. PMID: 27734822
4. Tabrizi S, Yeap BY, Sherman JC, et al. Long-term outcomes and late adverse effects of a prospective study on proton radiotherapy for patients with low-grade glioma. *Radiother Oncol*. 2019;137:95–101. doi:10.1016/j.radonc.2019.04.027
5. Taylor CW, Kirby AM. Cardiac side-effects from breast cancer radiotherapy. *Clin Oncol*. 2015;27(11):621–629. doi:10.1016/j.clon.2015.06.007
6. Ohta K, Murata H, Mori Y, et al. Remodeling of the tumor microenvironment by combined treatment with a novel radiosensitizer, {alpha}-sulfoquinovosylmonoacylglycerol ({alpha}-SQMG) and X-irradiation. *Anticancer Res*. 2010;30(11):4397–404. PMID: 21115885
7. Yagisawa T, Okumi M, Omoto K, Sawada Y, Morikawa S, Tanabe K. Novel approach for bladder cancer treatment using sulfoquinovosylacylpropanediol as a radiosensitizer. *Int J Urol*. 2016;23(3):270–272. doi:10.1111/iju.2016.23.issue-3
8. Yue WY, Clark JJ, Telisak M, Hansen MR. Inhibition of c-Jun N-terminal kinase activity enhances vestibular schwannoma cell sensitivity to gamma irradiation. *Neurosurgery*. 2013;73(3):506–516. doi:10.1227/01.neu.0000431483.10031.89
9. Davis RJ. Signal transduction by the JNK group of MAP kinases. *Cell*. 2000;103(2):239–252. doi:10.1016/S0092-8674(00)00116-1
10. Bode AM, Dong Z. The functional contrariety of JNK. *Mol Carcinog*. 2007;46(8):591–598. doi:10.1002/(ISSN)1098-2744
11. Lu C, Zhu F, Cho YY, et al. Cell apoptosis: requirement of H2AX in DNA ladder formation, but not for the activation of caspase-3. *Mol Cell*. 2006;23(1):121–132. doi:10.1016/j.molcel.2006.05.023
12. Weston CR, Davis RJ. The JNK signal transduction pathway. *Curr Opin Genet Dev*. 2002;12(1):14–21. doi:10.1016/S0959-437X(01)00258-1
13. Bulgin D, Podtcheko A, Takakura S, et al. Selective pharmacologic inhibition of c-Jun NH2-terminal kinase radiosensitizes thyroid anaplastic cancer cell lines via induction of terminal growth arrest. *Thyroid*. 2006;16(3):217–224. doi:10.1089/thy.2006.16.217
14. Kang YH, Lee SJ. Role of p38 MAPK and JNK in enhanced cervical cancer cell killing by the combination of arsenic trioxide and ionizing radiation. *Oncol Rep*. 2008;20(3):637–643. doi:10.3892/or_00000053
15. Kook SH, Son YO, Jang YS, et al. Inhibition of c-Jun N-terminal kinase sensitizes tumor cells to flavonoid-induced apoptosis through down-regulation of JunD. *Toxicol Appl Pharmacol*. 2008;227(3):468–476. doi:10.1016/j.taap.2007.11.004
16. An J, Chervin AS, Nie A, Ducoff HS, Huang Z. Overcoming the radioresistance of prostate cancer cells with a novel Bcl-2 inhibitor. *Oncogene*. 2007;26(5):652–661. doi:10.1038/sj.onc.1209830
17. Li CH, Lim SH, Ryu HH, Moon KS, Jung TY, Jung S. Enhancement of radiosensitivity by inhibition of c-Jun N-terminal kinase activity in a Lewis lung carcinomabearing subcutaneous tumor mouse model. *Oncol Rep*. 2016;36(6):3397–3404. doi:10.3892/or.2016.5204
18. Rizvi SAA, Saleh AM. Applications of nanoparticle systems in drug delivery technology. *Saudi Pharm J*. 2018;26(1):64–70. doi:10.1016/j.jsps.2017.10.012
19. Tiwari G, Tiwari R, Sriwastawa B, et al. Drug delivery systems: an updated review. *Int J Pharm Investig*. 2012;2(1):2–11. doi:10.4103/2230-973X.96920
20. Han L, Kong DK, Zheng MQ, et al. Increased nanoparticle delivery to brain tumors by autocatalytic priming for improved treatment and imaging. *ACS Nano*. 2016;10(4):4209–4218. doi:10.1021/acsnano.5b07573
21. Jain KK. A critical overview of targeted therapies for glioblastoma. *Front Oncol*. 2018;8:419. doi:10.3389/fonc.2018.00419
22. Saraiva C, Praca C, Ferreira R, Santos T, Ferreira L, Bernardino L. Nanoparticle-mediated brain drug delivery: overcoming blood-brain barrier to treat neurodegenerative diseases. *J Control Release*. 2016;235:34–47. doi:10.1016/j.jconrel.2016.05.044
23. Zong Z, Hua L, Wang Z, et al. Self-assembled angiopep-2 modified lipid-poly (hypoxic radiosensitized polyprodrug) nanoparticles delivery TMZ for glioma synergistic TMZ and RT therapy. *Drug Deliv*. 2019;26(1):34–44. doi:10.1080/10717544.2018.1534897
24. Hariri G, Yan H, Wang H, Han Z, Hallahan DE. Radiation-guided drug delivery to mouse models of lung cancer. *Clin Cancer Res*. 2010;16(20):4968–4977. doi:10.1158/1078-0432.CCR-10-0969

25. Hallahan DE, Qu S, Geng L, et al. Radiation-mediated control of drug delivery. *Am J Clin Oncol*. 2001;24(5):473–480. doi:10.1097/00000421-200110000-00012
26. Passarella RJ, Spratt DE, van der Ende AE, et al. Targeted nanoparticles that deliver a sustained, specific release of Paclitaxel to irradiated tumors. *Cancer Res*. 2010;70(11):4550–4559. doi:10.1158/0008-5472.CAN-10-0339
27. Han M, Wang H, Zhang HT, Han Z. The PDZ protein TIP-1 facilitates cell migration and pulmonary metastasis of human invasive breast cancer cells in athymic mice. *Biochem Biophys Res Commun*. 2012;422(1):139–145. doi:10.1016/j.bbrc.2012.04.123
28. Han M, Wang H, Zhang HT, Han Z. Expression of TIP-1 confers radioresistance of malignant glioma cells. *PLoS One*. 2012;7(9):e45402. doi:10.1371/journal.pone.0045402
29. Wang H, Yan H, Fu A, Han M, Hallahan D, Han Z. TIP-1 translocation onto the cell plasma membrane is a molecular biomarker of tumor response to ionizing radiation. *PLoS One*. 2010;5(8):e12051. doi:10.1371/journal.pone.0012051
30. Derfus AM, von Maltzahn G, Harris TJ, et al. Remotely triggered release from magnetic nanoparticles. *Adv Mater*. 2007;19(22):3932. doi:10.1002/(ISSN)1521-4095
31. Peppicelli S, Andreucci E, Ruzzolini J, et al. The acidic microenvironment as a possible niche of dormant tumor cells. *Cel Mol Life Sci*. 2017;74(15):2761–2771. doi:10.1007/s00018-017-2496-y
32. Lim SH, Jung S. inventors; Chonnam National University Hospital, assignee. Irradiation Device for Stereotactic Irradiation of Gamma-Rays and Experimental Method Thereof. Republic of korea Patent 1018223980000. 2018 Jan 22doi:10.8080/1020170016855.
33. Lim SH, Jung TY, Jung S, et al. Quantitative feasibility evaluation of ^{11}C-Methionine positron emission tomography images in gamma knife radiosurgery : phantom-based study and clinical application. *J Korean Neurosurg Soc*. 2019;62:476–486. doi:10.3340/jkns.2019.0104
34. Li S, Li C, Ryu HH, Lim SH, Jang WY, Jung S. Bacitracin inhibits the migration of U87-MG glioma cells via interferences of the integrin outside-in signaling pathway. *J Korean Neurosurg Soc*. 2016;59(2):106–116. doi:10.3340/jkns.2016.59.2.106
35. Jin SG, Ryu HH, Li SY, et al. Nogo-A inhibits the migration and invasion of human malignant glioma U87MG cells. *Oncol Rep*. 2016;35(6):3395–3402. doi:10.3892/or.2016.4737
36. Kim TW, Ryu HH, Li SY, et al. PDIA6 regulation of ADAM17 shedding activity and EGFR-mediated migration and invasion of glioblastoma cells. *J Neurosurg*. 2017;126(6):1829–1838. doi:10.3171/2016.5.JNS152831
37. Pei J, Park IH, Ryu HH, et al. Sublethal dose of irradiation enhances invasion of malignant glioma cells through p53-MMP 2 pathway in U87MG mouse brain tumor model. *Radiat Oncol*. 2015;10:164. doi:10.1186/s13014-015-0475-8
38. Han MS, Jang WY, Moon KS, et al. Is fractionated gamma knife radiosurgery a safe and effective treatment approach for large-volume (>10 cm(3)) intracranial meningiomas? *World Neurosurg*. 2017;99:477–483. doi:10.1016/j.wneu.2016.12.056
39. Hall EJ. *Radiobiology for the Radiologist*. 5th ed. Lippincott Williams & Wilkins; 2000.
40. Tai W, Mahato R, Cheng K. The role of HER2 in cancer therapy and targeted drug delivery. *J Control Release*. 2010;146(3):264–275. doi:10.1016/j.jconrel.2010.04.009
41. Wu AM, Senter PD. Arming antibodies: prospects and challenges for immunoconjugates. *Nat Biotechnol*. 2005;23(9):1137–1146. doi:10.1038/nbt1141
42. Lin PC, He JY, Le YY, et al. Radiation-guided peptide delivery in a mouse model of nasopharyngeal carcinoma. *Biomed Res Int*. 2016;2016:5382047. doi:10.1155/2016/5382047
43. Han SS, Li ZY, Zhu JY, et al. Dual-pH sensitive charge-reversal polypeptide micelles for tumor-triggered targeting uptake and nuclear drug delivery. *Small*. 2015;11(21):2543–2554. doi:10.1002/smll.201402865
44. Han Z, Fu A, Wang H, et al. Noninvasive assessment of cancer response to therapy. *Nat Med*. 2008;14(3):343–349. doi:10.1038/nm1691
45. Lowery A, Onishko H, Hallahan DE, Han Z. Tumor-targeted delivery of liposome-encapsulated doxorubicin by use of a peptide that selectively binds to irradiated tumors. *J Control Release*. 2011;150(1):117–124. doi:10.1016/j.jconrel.2010.11.006
46. Pridgen EM, Langer R, Farokhzad OC. Biodegradable, polymeric nanoparticle delivery systems for cancer therapy. *Nanomedicine*. 2007;2(5):669–680. doi:10.2217/17435889.2.5.669
47. Ashfaq UA, Riaz M, Yasmeen E, Yousaf MZ. Recent advances in nanoparticle-based targeted drug-delivery systems against cancer and role of tumor microenvironment. *Crit Rev Ther Drug Carrier Syst*. 2017;34(4):317–353. doi:10.1615/CritRevTherDrugCarrierSyst.v34.i4
48. Kim HJ, Kim A, Miyata K, Kataoka K. Recent progress in development of siRNA delivery vehicles for cancer therapy. *Adv Drug Deliv Rev*. 2016;104:61–77. doi:10.1016/j.addr.2016.06.011
49. Wickens JM, Alsaab HO, Kesharwani P, et al. Recent advances in hyaluronic acid-decorated nanocarriers for targeted cancer therapy. *Drug Discov Today*. 2017;22(4):665–680. doi:10.1016/j.drudis.2016.12.009
50. Qiao J, Dong P, Mu X, Qi L, Xiao R. Folic acid-conjugated fluorescent polymer for up-regulation folate receptor expression study via targeted imaging of tumor cells. *Biosens Bioelectron*. 2016;78:147–153. doi:10.1016/j.bios.2015.11.021
51. Danhier F, Feron O, Preat V. To exploit the tumor microenvironment: passive and active tumor targeting of nanocarriers for anti-cancer drug delivery. *J Control Release*. 2010;148(2):135–146. doi:10.1016/j.jconrel.2010.08.027
52. Chaurasiya B, Mahanty A, Roy D, Shen Y, Tu J, Sun C. Influence of tumor microenvironment on the distribution and elimination of nanoformulations. *Curr Drug Metab*. 2016;17(8):783–798. doi:10.2174/1389200217666160607093347
53. Chen D, Zhang G, Li R, et al. Biodegradable, hydrogen peroxide, and glutathione dual responsive nanoparticles for potential programmable paclitaxel release. *J Am Chem Soc*. 2018;140(24):7373–7376. doi:10.1021/jacs.7b12025
54. Hayward SL, Wilson CL, Kidambi S. Hyaluronic acid-conjugated liposome nanoparticles for targeted delivery to CD44 overexpressing glioblastoma cells. *Oncotarget*. 2016;7(23):34158–34171. doi:10.18632/oncotarget.v7i23
55. Lee HL, Hwang SC, Nah JW, et al. Redox- and pH-responsive nanoparticles release piperlongumine in a stimuli-sensitive manner to inhibit pulmonary metastasis of colorectal carcinoma cells. *J Pharm Sci*. 2018;107(10):2702–2712. doi:10.1016/j.xphs.2018.06.011
56. Mattheolabakis G, Milane L, Singh A, Amiji MM. Hyaluronic acid targeting of CD44 for cancer therapy: from receptor biology to nanomedicine. *J Drug Target*. 2015;23(7–8):605–618. doi:10.3109/1061186X.2015.1052072
57. Liu J, Huang Y, Kumar A, et al. pH-sensitive nano-systems for drug delivery in cancer therapy. *Biotechnol Adv*. 2014;32(4):693–710. doi:10.1016/j.biotechadv.2013.11.009
58. Ghassami E, Varshosaz J, Taymouri S. Redox sensitive polysaccharide based nanoparticles for improved cancer treatment: a comprehensive review. *Curr Pharm Des*. 2018;24(28):3303–3319. doi:10.2174/1381612824666180813114841
59. Zhao J, Yang Y, Han X, et al. Redox-sensitive nanoscale coordination polymers for drug delivery and cancer theranostics. *ACS Appl Mater Interfaces*. 2017;9(28):23555–23563. doi:10.1021/acsami.7b07535
60. Jeong GW, Jeong YI, Nah JW. Triggered doxorubicin release using redox-sensitive hyaluronic acid-g-stearic acid micelles for targeted cancer therapy. *Carbohydr Polym*. 2019;209:161–171. doi:10.1016/j.carbpol.2019.01.018

61. Raja MA, Arif M, Feng C, Zeenat S, Liu CG. Synthesis and evaluation of pH-sensitive, self-assembled chitosan-based nanoparticles as efficient doxorubicin carriers. *J Biomater Appl*. 2017;31(8):1182–1195. doi:10.1177/0885328216681184

62. van Vulpen M, Kal HB, Taphoorn MJ, El-Sharouni SY. Changes in blood-brain barrier permeability induced by radiotherapy: implications for timing of chemotherapy? (Review). *Oncol Rep*. 2002;9(4):683–688. PMID: 12066192